

Influence of Hot Isostatic Pressing on the Performance of Aluminum Alloy Fabricated by Ultrasonic Additive Manufacturing*

M. N. Gussev^{1*}, N. Sridharan^{1,2}, Z. Thompson¹, K. A. Terrani¹, S. S. Babu^{1,2}

¹ Oak Ridge National Laboratory, Oak Ridge, TN 37831

² University of Tennessee, Knoxville, TN 37916

*Corresponding author.

Postal address: MS-6151, PO Box 2008, Oak Ridge, TN 37831

Telephone number: (865) 574-4456

Fax number: (865) 574-6095

E-mail address: gussevmn@ornl.gov

Abstract

Ultrasonic additive manufacturing (UAM) is a solid-state additive manufacturing technique employing principles of ultrasonic welding coupled with mechanized tape layering to fabricate fully functional parts. However, UAM-fabricated parts often exhibit a reduction in strength when loaded normal to the welding interfaces (Z-direction). Here, the effect of hot isostatic pressing (HIP) on UAM builds of aluminum alloy was explored. Tensile testing and microstructure characterization were conducted; it was established that HIP eliminated the brittle Z-direction fracture and improved the strength and ductility of the Z-direction specimens. HIP eliminated voids and produced recrystallized structure; however, welding interfaces survived the HIP treatment.

Keywords

Ultrasonic additive manufacturing, hot isostatic pressing, electron back scatter diffraction, tensile tests.

* This manuscript has been authored by UT-Battelle, LLC under Contract No. DE-AC05-00OR22725 with the U.S. Department of Energy. The United States Government retains and the publisher, by accepting the article for publication, acknowledges that the United States Government retains a non-exclusive, paid-up, irrevocable, world-wide license to publish or reproduce the published form of this manuscript, or allow others to do so, for United States Government purposes. The Department of Energy will provide public access to these results of federally sponsored research in accordance with the DOE Public Access Plan (<http://energy.gov/downloads/doe-public-access-plan>).

Introduction

Ultrasonic additive manufacturing (UAM) is a novel, solid-state manufacturing process that uses ultrasonic vibrations to fabricate parts in layers [1–5]. In contrast to traditional manufacturing technologies, UAM allows for manufacturing complex parts with internal channels, cavities [3], or embedded elements made of different material(s) with special properties [6]. UAM can fabricate fully functional hybrid materials and parts by embedding fibers [7,8], wires, or sensors during the additive process. However, like other additive manufacturing techniques, the UAM products often exhibit anisotropic mechanical properties and demonstrate relatively low strength levels when loaded perpendicular to the welding layers [9] (often referred to as Z-direction). The low strength in the Z-direction (Z-strength) has generally been attributed to the presence of voids [10] and the lack of bonding between the layers [11].

Since low Z-strength levels limit the range of possible applications, several approaches have been developed to increase the UAM material's performance. The most obvious approach is to optimize the UAM process parameters [4,9,10,12–16], which provides significant benefits but has limitations for equipment performance. Bulk deformation methods (rolling, forging, etc.) may be applied to the additively manufactured components under some conditions [1], thereby reducing porosity and anisotropy to some degree. For many welding techniques, such as gas metal arc welding [17], gas tungsten arc welding [18], or stir welding [19], post-weld heat treatments (PWHT) may be beneficial for improving the weldment performance [17,18,20]. Recently, PWHTs have been used successfully to improve the performance of UAM materials [16,21,22]. For instance, a roughly 3.5× increase in Z-strength was seen in a UAM product after controlled PWHT [21].

While PWHT is an effective way to improve the mechanical properties of the UAM parts, further improvements are possible, for instance, through hot isostatic pressing (HIP). The advantages of using HIP for traditional welding techniques are well documented [23,24], and HIP offers a reduction in void fraction and improves the interface strength. One may expect that HIP will also be beneficial for the UAM-produced parts. However, there is limited, if any, literature on HIP's effect on UAM-produced components. The present work investigates the mechanical behavior and microstructure of a UAM-fabricated product made of an Al-6061 alloy that is subjected to HIP.

Experimental Work

Commercially available 150 μm Al-6061 H-18 alloy tapes were used in this study (see Table 1 for composition). The UAM builds were fabricated using the 9 kW UAM machine at Fabrisonic, LLC (Columbus, OH) [3]. The parameters used for fabrication included a vibration amplitude of 35 μm, normal force of 5,000 N, travel speed of 85 mm/s, and a preheating temperature maintained at 75 °C. The microstructural characterization and mechanical properties of the as-received (AR) material have been published elsewhere [25]. Additional information on microstructure and tensile behavior after conventional PWHT may be found in [21].

The HIP was conducted inside an AIP 6-30H system (American Isostatic Presses, Inc., Columbus, OH). The UAM blocks were placed inside an alumina crucible and subsequently positioned into the HIP unit's resistance heating furnace. The HIP treatment duration was 1 h, with a pressure of 100 MPa, and a maintained temperature of 580 °C. Note that the UAM blocks were not canned or sealed inside a leak resistant container before undergoing HIP.

Table 1. Alloy element compositions (wt. %)

Al	Mg	Si	Fe	Cu	Cr	Ti	Mn	Zn	Ni
Balance	0.86	0.66	0.35	0.23	0.13	0.084	0.082	0.077	0.015

Tensile dog-bone specimens with a dimension of $5 \times 1.2 \times 0.75$ mm were prepared using electro-discharge machining. Specimens were extracted from the AR blocks and from the HIP-treated blocks in three directions (Figure 1): X, along the direction of the travel of the sonotrode; Y, along the sonotrode vibration direction; and Z, along the build direction—with the load—applied normal to the interfaces.

Tensile tests were performed on an MTS Insight 2-52 one-column tensile screw machine. Five specimens in AR condition and three specimens that underwent HIP were tested in each direction. All specimens were shoulder loaded using special grips and tested at room temperature with a strain rate of 10^{-3} s^{-1} . To investigate the structure, specimens were mounted on cold mounting epoxy and prepared using standard metallography techniques. Following the polishing step, samples were examined using optical microscopy to check for voids, cracks, and other defects. Electron backscatter diffraction (EBSD) scanning and fractography analysis were performed on a JEOL 6500 FEG scanning electron microscope; the operational voltage varied in different tests from 10 kV to 20 kV, depending on grain size and magnification.

Results and Discussions

Figure 1 shows the typical structure of UAM specimens prior to and after HIP. In the AR material, the voids formed specific chains, which revealed the added material layers. In most cases, the void length was roughly 80–100 μm . As discussed in [25], the presence of voids was detrimental to the material's performance. Ductility was practically zero when loaded and tested in the Z-direction. PWHT, applied to the same material [21], allowed for increased Z-strength but did not improve Z-direction ductility nor did it influence the void structure. In contrast to the usual PWHT, voids fully disappeared from the structure after HIP. Optical microscopy revealed chains of precipitate particles along the former interfaces, Figure 1; however, no remaining voids, cavities, or pores were observed with optical microscopy or scanning electron microscopy. Void disappearance suggests that the voids were not interconnected and that the connection between the voids and the surface was limited. Otherwise, the pressure in the open voids would prevent their collapse.

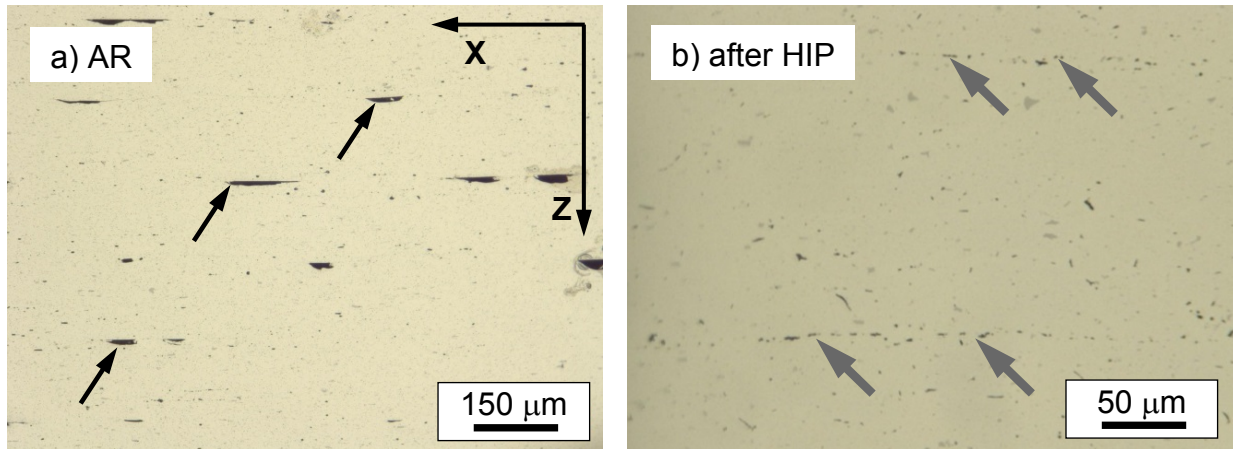


Figure 1. Structure of the UAM-produced material: a) as-received (AR); b) after HIP. Multiple voids (black arrows) are grouped along the welding interfaces in the AR alloy. However, after HIP, the material's structure is solid and void free. Former interfaces featuring precipitate particles are indicated by grey arrows. For coordinate system definition and additional detail see [21].

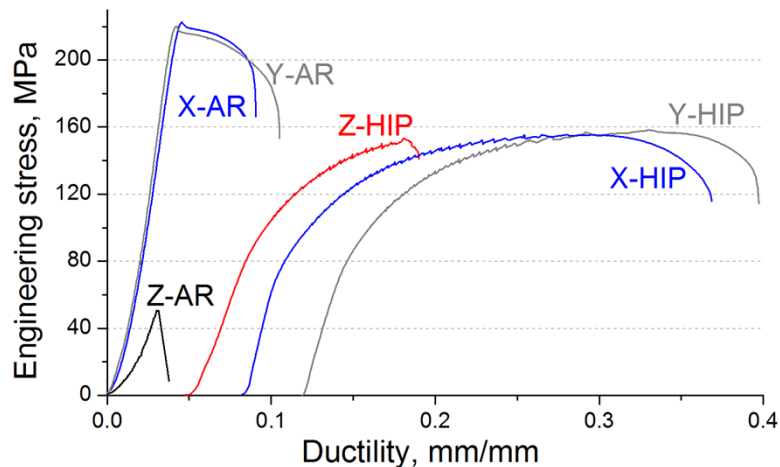


Figure 2. Representative engineering tensile curves for AR and HIP specimens. Note the significant improvement in the ductility for the Z-direction after HIP. Some curves are shifted along the X-axis to improve the image readability.

Figure 2 shows representative tensile curves for different conditions (AR vs. HIP), and Table 2 shows the summary mechanical test results. As shown in the results, the AR UAM X and Y specimens had relatively high strength, typical for cold worked conditions, and low ductility. The uniform deformation value was practically zero, and the necking initiated spontaneously after yield stress was reached. No force drops were observed on the tensile curves. When loaded normal to the interfaces (Z-direction), the Z-AR specimens showed practically zero ductility and had macroscopically brittle fracture behavior (Figure 2). The fracture stress did not exceed 50 MPa, which is roughly 20%–25% of the maximum load for the X and Y AR-specimens. Similar behavior was observed in [25]. PWHTs, offered and investigated in [21], improved the Z-

strength level; however, even full recrystallization and consequent aging did not improve ductility or eliminate brittle fracture for Z-direction specimens (Table 2).

After HIP, all UAM specimens (X, Y, and Z) had a yield stress of roughly 70–80 MPa and an ultimate stress on the order of 150–160 MPa. The drop in the yield strength can be attributed to the recrystallization and dissolution of any strengthening precipitates. Material strength values were slightly above the level expected for the bulk 6061 alloy in the annealed conditions. Appropriate solutionizing and aging heat treatments (e.g., T6 aging) may **additionally** improve the strength level **of the HIP-material**, and this question should be addressed in a separate work.

The most important result is the non-zero ductility and pronounced strain hardening for the Z-specimen after HIP; compare the tensile curves for Z-AR and Z-HIP specimens (Figure 2). Z-specimens after HIP demonstrated ductile behavior; however, the overall ductility level fell below the typical values for X and Y specimens.

For the HIP samples, the tensile curves showed pronounced force drops (~3–5 MPa in amplitude) and serrated flow. The load drops could be a result of the Portevin-Le-Chatelier (PLC) effect [26–28]. As is generally accepted, the main cause for the PLC effect is the interaction of solute atoms with dislocations [26,27], and the phenomenon strongly depends on test temperature, prior heat treatments, and strain rate. The effect is very pronounced in the solutionized state since the solute atoms are in solid solution, which results in the interaction between the solute and dislocations. Based on the stress-strain curve and more-or-less regular force drop character, it was concluded that the force drops were caused by type A deformation bands, where the bands nucleate near the specimen head and propagate along the gauge [27]. However, detailed analysis of the PLC effect is beyond the scope of the present work.

Table 2. Mechanical properties of UAM-fabricated alloy before and after HIP

Material	Direction	Yield stress, MPa	Ultimate stress, MPa	Uniform elongation, %	Total elongation, %
UAM (AR)	X	217	225	1.1	5.1
	Y	221	223.7	0.5	6.0
	Z	46.2*	–	–	–
PWHT**	X	254.3	313.0	10.1	14.4
	Y	259.7	315.4	10.6	13.6
	Z	177.6	–	–	–
After HIP	X	70	158	17.3	27.3
	Y	78	159	17.0	26.4
	Z	80	151	7.9	11.5

* Fracture stress.

** Annealing at 580 °C for 1h, followed by aging at 180 °C for 8h (see [21]).

The results from the mechanical tests show that subjecting the UAM builds to HIP offered significant improvements in (increased) ductility. HIP also changed the fracture mechanism; in the AR material, fracture occurred via delamination of the tapes when loaded in the Z-direction, Figure 3 (left).

Cracks initially nucleated near the regions of pre-existing strain localizations [25] and voids (hence it underwent cleavage) and propagated along the interface region [25]. The cross-section analysis also showed multiple internal cracks that appeared far from the fracture location and propagated along the interfaces.

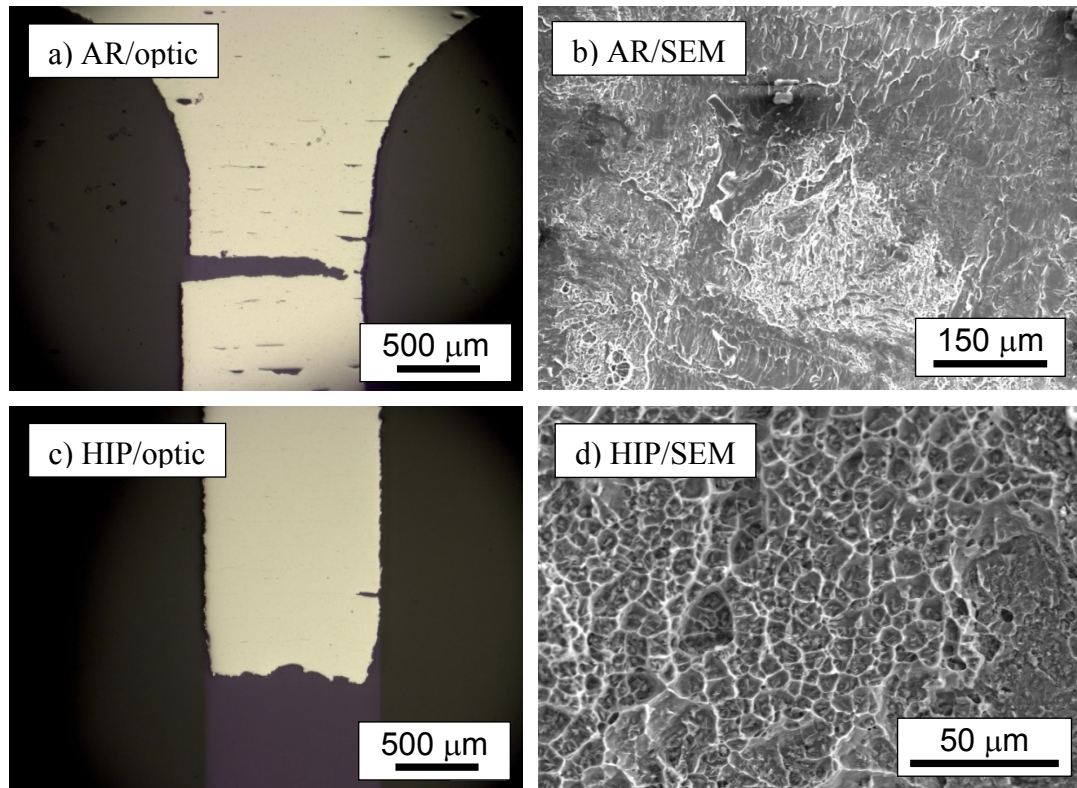


Figure 3. Fracture mechanisms in Z-tensile specimens before (a, b) and after (c, d) HIP. More information on the AR state is given in [25].

In contrast, the deformed and fractured HIP Z specimens demonstrated solid, practically void-free structure. In very rare cases, small secondary cracks appeared near the tensile specimen edge after deformation. Figure 3 shows the optical micrograph of the tested specimens' cross section; unlike the AR Z-specimen that had delamination and multiple internal cracks, the material that underwent HIP did not demonstrate internal cracks. Fractures in the HIP-treated material developed in bulk and the specimen did not fail by delamination. The fracture surface demonstrated a ductile fracture mechanism with multiple dimples (Figure 3d). The tested HIP Z specimens revealed significant area reduction and neck geometry typical for the bulk material. For the X and Y specimens that underwent HIP, the fracture surface (not shown) always revealed a ductile fracture surface typical for bulk alloy. The pronounced layered structure, observed in the AR UAM X and Y specimens [21,25], disappeared with HIP.

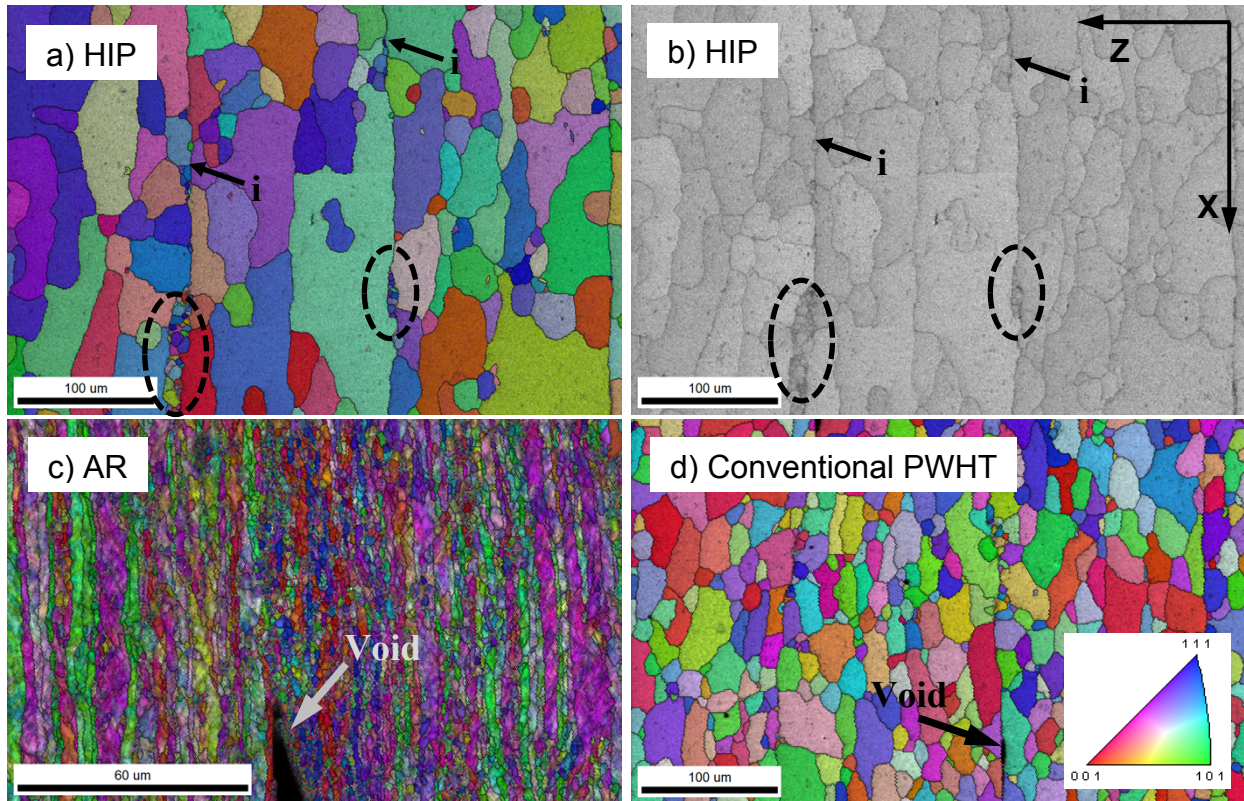


Figure 4. a) EBSD IPF map (colored in the Z-direction) for specimen after HIP. b) IQ map HIP (same location). Black arrows point to welding interface locations (i). Dashed ovals show the groups of small grains. X and Z show the orientation of the specimen during the UAM-process [21,25]. c) IPF map for the AR-material [25]. d) IPF-map for the alloy subjected to a conventional PWHT [21] (annealing at 580 °C for 1 h and aging at 180 °C for 8 h). Note the voids in the structure of the non-HIP material.

As observed in the cross-section analysis, Figure 3 (right), the HIP-induced strength and ductility enhancement was driven by the void disappearance. Since no cavities appeared in the HIP Z specimen during tension, one may speculate that void closure, along with some additional bonding between the former void edges, strengthened the interfaces. Additionally, based on the mechanical property evaluation, recrystallization may be expected. EBSD analysis was performed to understand the effect of HIP on the microstructure.

The EBSD data, presented in Figure 4, shows the microstructure of UAM HIP material. One can see that significant structural transformation and grain growth took place because of elevated temperature. The AR-microstructure was almost completely removed. The new grains had a rounded shape that was often elongated in the X direction.

Interestingly, the original interfaces between tapes survived the HIP treatment and were still clearly visible. Interface-adjacent areas experienced recrystallization, but no grain growth across the interfaces was observed. At the same time, the ductile fracturing that occurred far from the interfaces in the HIP Z specimens suggests that the fine interface structure was different when compared to the AR material.

Interestingly, conventional PWHT (annealing at 580 °C for 1 h and aging at 180 °C for 8 h [21]), when applied to the same material, eliminated about half of the interfaces. This observation points out that recrystallization processes and grain structure evolution may be sensitive to the applied pressure. It also suggests the possibility of complex treatments, where HIP is used to close voids and annealing is used to eliminate interfaces, followed by final aging. This possibility will be addressed in future work. While grain growth occurred in the interface-adjacent areas, there are certain regions that were surprisingly stable and kept their small grain structure during both HIP and conventional PWHT. To date, this stability is not yet fully understood and requires further analysis [29].

Conclusions

The present work offered a novel experimental approach (HIP under controlled conditions) to improving the performance of the parts and components produced by UAM. HIP eliminated structural voids in the UAM products, and the Z-direction specimens subjected to HIP appeared to be ductile, with a pronounced neck forming prior the fracture. Interestingly, the welding interfaces survived the HIP treatment. Further improvement in the properties may be achieved by combining HIP with conventional treatments like aging.

Acknowledgments

This work was sponsored by the Laboratory Directed Research and Development program at Oak Ridge National Laboratory (ORNL). EBSD analysis was performed at ORNL's Center for Nanophase Materials. The authors would like to thank Dr. A. Hehr (Fabrisonic, LLC) for fruitful comments and discussion and S. Crawford (ORNL) for help with manuscript preparation.

References

- [1] P.A. Colegrove, J. Donoghue, F. Martina, J. Gu, P. Prangnell, and J. Hönnige, "Application of bulk deformation methods for microstructural and material property improvement and residual stress and distortion control in additively manufactured components," *Scripta Materialia*, 2016.
- [2] H.T. Fujii, S. Shimizu, Y.S. Sato, and H. Kokawa, "High-strain-rate deformation in ultrasonic additive manufacturing," *Scripta Materialia*, 2017.
- [3] M. Norfolk and H. Johnson, "Solid-state additive manufacturing for heat exchangers," *JOM*, vol. 67, 2015, pp. 655–659.
- [4] S. Shimizu, H.T. Fujii, Y.S. Sato, H. Kokawa, M.R. Sriraman, and S.S. Babu, "Mechanism of weld formation during very-high-power ultrasonic additive manufacturing of Al alloy 6061," *Acta Materialia*, vol. 74, 2014, pp. 234–243.
- [5] P.J. Wolcott, A. Hehr, and M.J. Dapino, "Optimized welding parameters for Al 6061 ultrasonic additive manufactured structures," *Journal of Materials Research*, vol. 29, 2014, pp. 2055–2065.
- [6] A. Hehr, J. Wenning, K. Terrani, S.S. Babu, and M. Norfolk, "Five-Axis Ultrasonic Additive Manufacturing for Nuclear Component Manufacture," *JOM*, 2016, pp. 1–6.

- [7] D. Li and R.C. Soar, "Plastic flow and work hardening of Al alloy matrices during ultrasonic consolidation fibre embedding process," *Materials Science and Engineering: A*, vol. 498, 2008, pp. 421–429.
- [8] J. Li, T. Monaghan, S. Masurtschak, A. Bournias-Varotsis, R.J. Friel, and R.A. Harris, "Exploring the mechanical strength of additively manufactured metal structures with embedded electrical materials," *Materials Science and Engineering: A*, vol. 639, 2015, pp. 474–481.
- [9] D. Schick, R. Hahnlen, R. Dehoff, P. Collins, S. Babu, M. Dapino, and J. Lippold, "Microstructural Characterization of Bonding Interfaces in Aluminum 3003 Blocks Fabricated by Ultrasonic Additive Manufacturing-Methods were examined to link microstructure and linear weld density to the mechanical properties of ultrasonic additive manufacturing," *Welding Journal*, vol. 89, 2010, p. 105S.
- [10] G.J. Ram, Y. Yang, and B. Stucker, "Effect of process parameters on bond formation during ultrasonic consolidation of aluminum alloy 3003," *Journal of Manufacturing Systems*, vol. 25, 2006, pp. 221–238.
- [11] A.G. Truog, "Bond improvement of Al/Cu joints created by very high power ultrasonic additive manufacturing," The Ohio State University, 2012.
- [12] C. Hopkins, M. Dapino, and S. Fernandez, "Statistical characterization of ultrasonic additive manufacturing Ti/Al composites," *Journal of Engineering Materials and Technology*, vol. 132, 2010, p. 041006.
- [13] C. Kong, R. Soar, and P. Dickens, "Optimum process parameters for ultrasonic consolidation of 3003 aluminium," *Journal of materials processing technology*, vol. 146, 2004, pp. 181–187.
- [14] C. Kong, R. Soar, and P. Dickens, "Characterisation of aluminium alloy 6061 for the ultrasonic consolidation process," *Materials Science and Engineering: A*, vol. 363, 2003, pp. 99–106.
- [15] K. Sojiphan, "Effects of Very High Power Ultrasonic Additive Manufacturing Process Parameters on Hardness, Microstructure, and Texture of Aluminum 3003-H18 Alloy," The Ohio State University, 2015.
- [16] P. Wolcott, A. Hehr, C. Pawlowski, and M. Dapino, "Process improvements and characterization of ultrasonic additive manufactured structures," *Journal of Materials Processing Technology*, vol. 233, 2016, pp. 44–52.
- [17] R. Ahmad and M. Bakar, "Effect of a post-weld heat treatment on the mechanical and microstructure properties of AA6061 joints welded by the gas metal arc welding cold metal transfer method," *Materials & Design*, vol. 32, 2011, pp. 5120–5126.
- [18] M.W. Dewan, J. Liang, M. Wahab, and A.M. Okeil, "Effect of post-weld heat treatment and electrolytic plasma processing on tungsten inert gas welded AISI 4140 alloy steel," *Materials & Design*, vol. 54, 2014, pp. 6–13.
- [19] B. Wang, R. Ma, J. Zhou, Z. Li, S. Zhao, and X. Huang, "Adiabatic shear localization in ultrafine grained 6061 aluminum alloy," *Materials Science and Engineering: A*, vol. 675, 2016, pp. 221–227.
- [20] M. Temmar, M. Hadji, and T. Sahraoui, "Effect of post-weld aging treatment on mechanical properties of Tungsten Inert Gas welded low thickness 7075 aluminium alloy joints," *Materials & Design*, vol. 32, 2011, pp. 3532–3536.

- [21] M.N. Gussev, N. Sridharan, M. Norfolk, K.A. Terrani, and S.S. Babu, “Effect of post weld heat treatment on the 6061 aluminum alloy produced by ultrasonic additive manufacturing,” *Materials Science and Engineering: A*, vol. 684, 2017, pp. 606–616.
- [22] P.J. Wolcott, “Ultrasonic Additive Manufacturing: Weld Optimization for Aluminum 6061, Development of Scarf Joints for Aluminum Sheet Metal, and Joining of High Strength Metals,” The Ohio State University, 2015.
- [23] M. Agarwala, D. Bourell, J. Beaman, H. Marcus, and J. Barlow, “Post-processing of selective laser sintered metal parts,” *Rapid Prototyping Journal*, vol. 1, 1995, pp. 36–44.
- [24] X. Zhao, X. Lin, J. Chen, L. Xue, and W. Huang, “The effect of hot isostatic pressing on crack healing, microstructure, mechanical properties of Rene88DT superalloy prepared by laser solid forming,” *Materials Science and Engineering: A*, vol. 504, 2009, pp. 129–134.
- [25] N. Sridharan, M. Gussev, R. Seibert, C. Parish, M. Norfolk, K. Terrani, and S.S. Babu, “Rationalization of anisotropic mechanical properties of Al-6061 fabricated using ultrasonic additive manufacturing,” *Acta Materialia*, vol. 117, 2016, pp. 228–237.
- [26] P. Cetlin, A. Güleç, and R. Reed-Hill, “Serrated flow in aluminum 6061 alloy,” *Metallurgical Transactions*, vol. 4, 1973, pp. 513–517.
- [27] H. Jiang, Q. Zhang, X. Chen, Z. Chen, Z. Jiang, X. Wu, and J. Fan, “Three types of Portevin–Le Chatelier effects: experiment and modelling,” *Acta materialia*, vol. 55, 2007, pp. 2219–2228.
- [28] M.R. Rezaei, M.R. Toroghinejad, and F. Ashrafizadeh, “Effects of {ARB} and ageing processes on mechanical properties and microstructure of 6061 aluminum alloy,” *Journal of Materials Processing Technology*, vol. 211, 2011, pp. 1184–1190.
- [29] N. Sridharan, M. Gussev, C. Parish, D. Isheim, D. Seidman, K. Terrani, and S.S. Babu, “Evaluation of microstructure stability at the interfaces of Al-6061 welds fabricated using ultrasonic additive manufacturing,” *Acta Materialia (submitted)*.